Editors' Suggestion

# Local and Nonlocal Electronic Correlations at the Metal-Insulator Transition in the Two-Dimensional Hubbard Model

Maria Chatzieleftheriou,[1] Silke Biermann,[1,2,3] and Evgeny A. Stepanov[1,2]
[1]CPHT, CNRS, École polytechnique, Institut Polytechnique de Paris, 91120 Palaiseau, France
[2]Collège de France, 11 place Marcelin Berthelot, 75005 Paris, France
[3]European Theoretical Spectroscopy Facility, 91128 Palaiseau, France

(Received 5 December 2023; accepted 13 May 2024; published 5 June 2024)

Elucidating the physics of the single-orbital Hubbard model in its intermediate-coupling regime is a key missing ingredient to our understanding of metal-insulator transitions in real materials. Using recent nonperturbative many-body techniques that are able to interpolate between the spin-fluctuation-dominated Slater regime at weak coupling and the Mott insulator at strong coupling, we obtain the momentum-resolved spectral function in the intermediate regime and disentangle the effects of antiferromagnetic fluctuations and local electronic correlations in the formation of an insulating state. This allows us to identify the Slater and Heisenberg regimes in the phase diagram, which are separated by a crossover region of competing spatial and local electronic correlations. We identify the crossover regime by investigating the behavior of the local magnetic moment, shedding light on the formation of the insulating state at intermediate couplings.

DOI: 10.1103/PhysRevLett.132.236504

Ever since the seminal works by Slater [1] and Mott [2], correlation-induced metal-insulator transitions (MITs) in transition metal compounds such as vanadates, titanates, cuprates, or nickelates have intrigued the condensed matter and materials science community. The Hubbard model, a single-orbital lattice model describing the interplay of kinetic energy and Coulomb interactions, is a minimal model for such a MIT and has become the *Drosophila* of the field. While in the limiting cases of one and infinite spatial dimensions the exact solutions of the Hubbard model are known, the nature of the MIT in finite dimensions (and, in particular, in the important case of the model on the $d = 2$ square lattice) is still a subject of intense debate. In the weak-coupling regime, the half filled Hubbard model with nearest-neighbor hopping amplitudes undergoes a Néel transition to an antiferromagnetic (AFM) insulating state at a critical temperature $T_N$. In this Slater regime [1,3], the formation of the insulating state is driven by Fermi surface (FS) nesting, enabling fluctuations between FS points that are connected by the AFM wave vector. In the opposite—strong-coupling—limit, strong local Coulomb interaction localizes the electrons, inducing a Mott insulating state [2,4] with Heisenberg-type magnetic moments [5–9]. Upon decreasing temperature, at $T_N$ a Mott insulator undergoes a paramagnetic-to-AFM transition, which is no longer driven by the FS nesting, as the FS is absent in the Mott phase. Close to the paramagnetic Mott transition, the theoretical challenge consists of solving, at least approximately, the quantum many-body problem in the intermediate-coupling regime that cannot be reached by perturbative expansions around the weak-coupling (band) or strong-coupling (localized) limits. Moreover, in the proximity of the phase transition, long correlation lengths are expected, calling for techniques going beyond the local picture of dynamical mean field theory (DMFT) [10] methods.

Recent years have seen the development of a flurry of attempts in this direction, including "cluster" methods, where spatial (rather short-range) correlations are taken into account within a cluster of lattice sites [11–19], and "diagrammatic" methods, where nonlocal correlations are treated via a diagrammatic expansion around DMFT [20,21], such as $GW$ + DMFT [22–28], dual fermions [29–34], dual bosons [35–41], the dynamical vertex approximation [42–46], the triply irreducible local expansion (TRILEX) [47–50], or the dual TRILEX (D-TRILEX) [51–53] methods. In the weak-coupling regime, diagrammatic Monte Carlo [54–58] studies of the Hubbard model on the 2D square lattice [59–61] provide the numerically exact solution, evidencing characteristic momentum-selective effects stemming from AFM fluctuations as expected in the Slater regime. In the intermediate-coupling regime, however, and despite considerable progress in recent years, there is still no complete picture of the physics of even the single-orbital model at half filling.

In this Letter, we elucidate the spectral properties close to and the nature of the Mott transition in the half filled Hubbard model. We analyze corrections to the momentum-resolved spectral functions from nonlocal fluctuations taken into account beyond DMFT using D-TRILEX, disentangling the contribution of AFM fluctuations and local electronic correlations. We find the weak- and strong-

 

coupling limits to be separated by a crossover regime that starts when the local magnetic moment (LMM) is formed and ends at the Mott transition. In this regime, spatial fluctuations are important, but emergent LMMs herald strong local electronic correlations in the Mott phase. Increasing $U$ enhances the value of the LMM and concomitantly reduces the momentum selectivity of spectral features on the FS until it eventually disappears upon entering the Mott phase. Our Letter bridges the weak- and strong-coupling pictures of the MIT by providing a complete analysis of the interplay of nesting, local moment physics and Mott localization in the 2D Hubbard model.

We study the single-orbital half filled Hubbard model [62]: $\hat{H} = t\sum_{\langle jj'\rangle,\sigma} c^{\dagger}_{j\sigma}c_{j'\sigma} + U\sum_i n_{j\uparrow}n_{j\downarrow}$, on a 2D square lattice with dispersion $\epsilon_{\mathbf{k}} = 2t(\cos k_x + \cos k_y)$ and the on-site Coulomb interaction $U$. We use the half bandwidth as our unit of energy, i.e., $t = 0.25$. Here, $c^{(\dagger)}_{\sigma}$ is the annihilation (creation) operator for an electron with spin $\sigma \in \{\uparrow, \downarrow\}$ and $n_{j\sigma} = c^{\dagger}_{j\sigma}c_{j\sigma}$.

We solve the problem using the D-TRILEX approach [51–53] that allows for a self-consistent treatment of the local correlations and spatial charge and spin fluctuations of arbitrary range in different lattice geometries [63–70]. This method performs a diagrammatic expansion on the basis of a generic interacting reference system [34], e.g., a DMFT impurity problem as used in this Letter. This expansion is performed in terms of new fermionic and bosonic variables that are dual to the original electronic degrees of freedom. In this way, D-TRILEX becomes perturbative around the exact weak- and strong-coupling limits.

The momentum-resolved spectral function $A(\mathbf{k},\omega) = -(1/\pi)\mathrm{Im}G(\mathbf{k},\mathbf{E})$ and its momentum-integrated (local) counterpart $\rho(\omega) = \sum_{\mathbf{k}} A(\mathbf{k},\omega)$ are obtained by performing analytical continuation for the Matsubara electronic Green's function $G(\mathbf{k},\nu)$ using the maximum entropy method implemented in the ANA_CONT package [71]. The spin susceptibility in D-TRILEX is given by a Bethe-Salpeter equation (BSE) [53] which, in the single-band case, reduces to the Dyson equation. The D-TRILEX calculations are performed in the normal (non-symmetry-broken) phase. In this case the formation of the ordered phase is captured by the divergence of the corresponding susceptibility when the "leading eigenvalue" $\lambda$ of the BSE approaches 1. We will use the value of $\lambda$ as a proxy for AFM fluctuations. To determine the role of nonlocal electronic correlations we compare the D-TRILEX results to the paramagnetic DMFT solution of the problem (given in Supplemental Material [72]).

Figure 1 displays the $\mathbf{k}$-resolved spectral function along a high-symmetry path in the Brillouin zone and its local counterpart in the high- (top row) and low-temperature (bottom row) regimes for three values of the interaction. At the high temperature, with increasing interaction strength—from left to right—the system evolves from a weakly correlated metal, with a spectral function resulting from the noninteracting one by mere temperature broadening, to a Mott insulator, where the Mott gap results from a splitting of the spectral features into upper and lower Hubbard bands, separated by the Hubbard interaction $\sim U$, as expected. In spite of the gap being well visible in the momentum-resolved spectral function, in the local spectral function, the strong thermal fluctuations at this temperature lead merely to a minimum of the spectral weight at the Fermi energy ($E_F$), rather than vanishing spectral weight (a similar result was observed in [75]). Results for these same parameters within DMFT are plotted in Supplemental Material [72]. The comparison of the D-TRILEX and DMFT results allows for a direct assessment of the role of nonlocal electronic correlations. As expected, at high temperatures, differences between D-TRILEX and DMFT

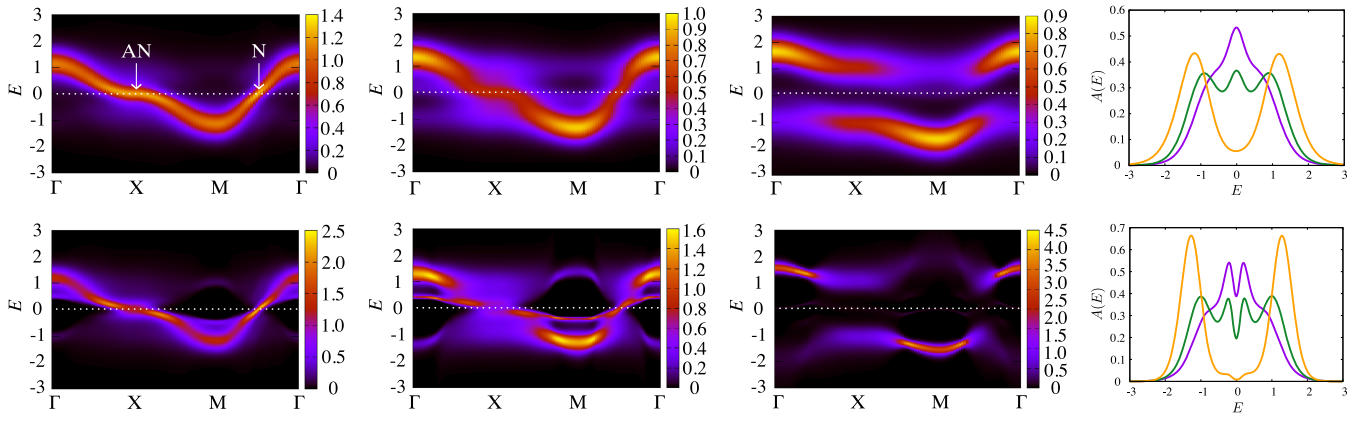


FIG. 1. Momentum-resolved spectral function of the Hubbard model at half filling, at $T = 0.14$ (upper row) and $T = 0.06$ (lower row) within D-TRILEX, at $U = 1.2$ (left), $U = 1.6$ (middle), and $U = 2.4$ (right), along the $k$ path $\Gamma - X - M - \Gamma$ with $\Gamma = (0,0)$, $X = (\pi,0)$, and $M = (\pi,\pi)$. The far right column displays the corresponding local spectral functions obtained for $U = 1.2$ (purple), $U = 1.6$ (green), and $U = 2.4$ (orange).

spectra are minor. Nonlocal magnetic fluctuations are negligible in this regime, as also confirmed by the spin leading eigenvalue being significantly smaller than $\lambda = 1$ (typically here $\lambda < 0.5$). In this regime, the MIT is thus driven by purely local Mott physics and DMFT is sufficient for addressing the problem.

The picture changes radically when cooling down. While within DMFT temperature-induced changes of the spectral function are minor and amount to a mere reduction of the width of the different spectral features, D-TRILEX unravels strongly temperature-dependent changes in the spectra. At the largest interaction studied, vanishing spectral weight at the Fermi level confirms the opening of the Mott gap, both in DMFT and D-TRILEX. Nevertheless, even at this relatively strong interactions, qualitative differences are observed between the purely local picture of DMFT and the D-TRILEX result. The differences in the local spectral functions can be traced back to the differences in the $\mathbf{k}$-resolved ones (see bottom row in Fig. 1). We observe, in particular, an overestimation of the widths of the Hubbard bands within DMFT, while D-TRILEX displays sharper excitations. Furthermore, within D-TRILEX, a "mirroring" phenomenon of the electronic dispersion with respect to zero energy sets in. Such a mirroring results from the proximity of the system to an ordered AFM state. Indeed, band backfoldings are a trivial effect occurring when the unit cell is doubled by some kind of ordering, e.g., of AFM nature. Here, they appear in a nontrivial way, from AFM fluctuations in the paramagnetic phase. Remarkably, within D-TRILEX, the mirroring of the bands is obtained purely diagrammatically, as calculations are performed using a single-site reference problem without any doubling of the unit cell. The strong AFM fluctuations are encoded in the nonlocal parts of the self-energy. We rationalize this behavior in Supplemental Material [72]. The mirroring of the bands is noticeable already at $U = 1.2$ (bottom left panel in Fig. 1) when the fluctuations are already relatively strong ($\lambda = 0.89$) and is well pronounced at $U = 1.6$ (middle panel), when the leading eigenvalue of magnetic fluctuations approaches unity ($\lambda = 0.94$). Further increase of the interaction to $U = 2.4$ results in the Mott transition, and the mirrored dispersion transforms into the two Hubbard bands (right panel).

The spectral functions close to $E_F$ reveal characteristic $\mathbf{k}$-dependent features. Already at $U = 1.2$ (bottom left panel) we observe a depletion of the spectral weight around the antinodal [$\mathrm{AN} = \mathrm{X} = (\pi, 0)$] point, while the nodal [$\mathrm{N} = (\pi/2, \pi/2)$] point remains unaffected. In the local spectral function, the reduction of the spectral weight at the AN point results in a minimum at the Fermi level. When increasing the interaction strength to $U = 1.6$, the quasiparticle (QP) peak at $E_F$ completely disappears at the AN point, but remains at the N point. This is a well-known effect of AFM fluctuations in the formation of an insulating state, which implies that the gap in the spectral function first opens at the AN point (middle panel at the bottom row), then propagates along the FS, and finally opens at the N point. Comparison of the momentum-resolved spectral functions from D-TRILEX, displayed in the bottom row of Fig. 1, is suggestive of an interpretation of the spectral function in the intermediate-coupling regime as a superposition of (mirrored) high-energy Hubbard bands and a low-energy QP band split by AFM fluctuations.

Inspection of the local spectral functions for the two lowest interaction values in the light of the $\mathbf{k}$-resolved spectra, calls for an important caveat: obviously, from the depletion of the local spectral weight at the Fermi level, one cannot establish insulating behavior of the system. Indeed, in the presence of nonlocal correlations, the local spectral function is no longer the appropriate quantity to look at, since a metallic regime with a momentum-selectively-gapped Fermi surface may not be distinguished from a thermally broadened insulator.

The observed momentum-selective disappearance of the quasiparticle peak at $E_F$ along the FS suggests to revisit the phase diagram and study the spectral function at the AN and N points separately. In Fig. 2, we regroup different pieces of information: The dark red line corresponds to the $(T, U)$ values for which the spin susceptibility at wave vector $\mathbf{q} = (\pi, \pi)$ diverges, indicating the Néel transition to the AFM (quasi)ordered state at lower $T$. Concomitantly, in the spectral function, at the N point, the QP peak at $E_F$ is lost, and a gap opens. The dark blue line depicts the

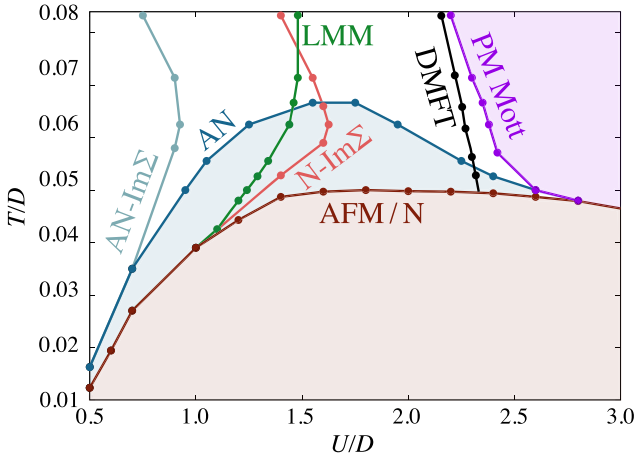


FIG. 2. Low-temperature phase diagram of the 2D Hubbard model within D-TRILEX. The different lines have been determined as follows: Divergence of the spin susceptibility at $\mathbf{q} = (\pi, \pi)$ (dark red line); sign change of the slope of the self-energy at the AN point (light blue curve); gap opening in the spectral function at the AN point (dark blue curve); sign change of the slope of the self-energy at the N point (light red curve); formation of nonzero local magnetic moment (green curve). The purple line corresponds to the simultaneous disappearance of the quasiparticle peak at $E_F$ for both N and AN points, identified with the paramagnetic (PM) Mott transition. The black curve is the equivalent result from single-site DMFT calculations.

formation of a minimum at $E_F$ in the spectral function at the AN point, which—as seen above—occurs at larger temperatures than at the N point. Interestingly, the AN curve (dark blue line) has a domelike shape mimicking the form of the Néel phase boundary. At $U \simeq 2.8$ the AN and N curves coincide, and the disappearance of the quasiparticle peak at $E_F$ is not momentum selective anymore in the regime of large interactions $U \gtrsim 2.8$. Remarkably, the form of the dark blue curve suggests that at certain values of $T$ by *increasing* the interaction strength $U$ one can move the system from the regime where part of the FS is gapped (blue area in Fig. 2) to a metallic regime (white area between the dark blue and purple curves), where QPs are restored along the entire FS. An example is given in Fig. 3.

Increasing the interaction even more results in a simultaneous disappearance of the QP peak at $E_F$ and in the formation of the gap at both AN and N points [Fig. 3(d)], which is depicted in Fig. 2 by the purple line. In the low-temperature regime, the purple curve goes toward larger values of $U$ upon decreasing temperature, until it eventually merges with the AN (dark blue) and N (dark red) lines. Remarkably, this simultaneous opening of the gap along the FS is non-momentum-selective and is thus governed by local electronic correlations. For this reason, we identify the purple curve with the Mott transition. Thus, in the regime of weak-to-intermediate interactions, AFM fluctuations highly affect the behavior of the system, introducing momentum selectivity between the N and AN points, which results in the momentum-selective disappearance of the quasiparticle peak along the FS. This behavior is consistent with a Slater-like scenario for the MIT. On the contrary, at strong interactions, local electronic correlations dominate.

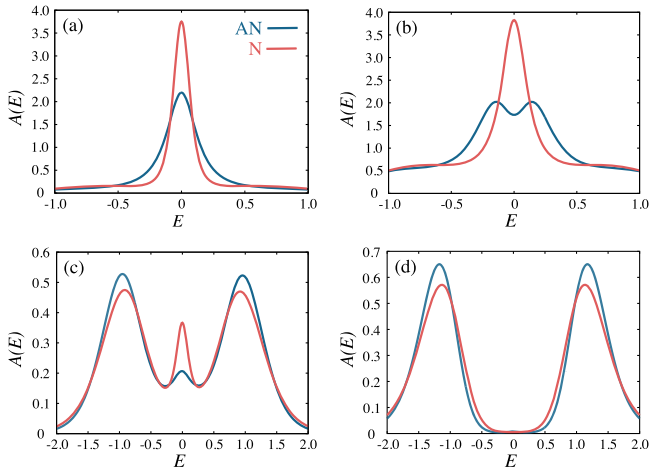


FIG. 3. Spectral function at the AN (red) and N (blue) points at $T = 0.062$ for $U = 1.0$ (a), $U = 1.4$ (b), $U = 2.0$ (c), and $U = 2.6$ (d). For increasing $U$, the QP peak at $E_F$ disappears first at the AN point, but is restored at larger values of $U$. Finally, the spectra are gapped at both points.

Interestingly, when taking into account nonlocal correlations, the paramagnetic Mott transition is actually realized at slightly larger values of $U$ than in single-site DMFT (see black and purple curves in Fig. 2). This is in contrast to results obtained within cluster DMFT methods [17,19], which find a reduction of $U_c$ for the Mott transition compared to single-site DMFT. This result, however, was obtained in these studies by analyzing either the local spectral function, the double occupancy, or the self-energy. These quantities embody a combined effect of temperature, magnetic fluctuations, and local correlations, and separating them is not a trivial task. Here we disentangle these two mechanisms and associate the Mott transition to an effect driven by the local correlations. An increase of $U_c$ was also discussed using TRILEX [48], based, however, on an analysis of the local spectral function at the Fermi energy, which—for the reasons explained above—is not a good quantity for determining the MIT.

How does the system interpolate between the two regimes of dominant spatial and local electronic correlations? The first signature of the crossover between the two regimes is the decrease of the N-AN dichotomy at $U \gtrsim 1.5$, which manifests itself in a decrease of the difference between the critical temperatures for the disappearance of the quasiparticle peak at $E_F$ at the AN and N points (dark blue and red lines in Fig. 2). This means that the local electronic correlations start to take over the spatial ones well before the system undergoes the Mott transition.

Also plotted in Fig. 2 are the critical values ($T$, $U$) at which the behavior of the self-energy at the AN (light blue) and N (light red line) points changes from metallic Fermi-liquid-like to incoherent and eventually gapped behavior. The self-energies themselves are plotted in Supplemental Material [72]. In the weak-coupling regime, the dark and light red curves coincide with the disappearance of the QP peak at the N point. However, at $U > 1$ and $T \simeq 0.38$ the light red curve exhibits a turn toward a smaller value of interactions once the temperature increases. A similar behavior is observed for the light blue curve, which starts deviating from the dark blue curve at a similar temperature $T \simeq 0.38$. Such a trend has also been detected in the diagrammatic Monte Carlo study [58,76] in the same regime of weak-to-intermediate correlations.

For this regime of increasing interactions, the low-frequency behavior of the self-energy is obviously no longer a good proxy for the behavior of the system, where local correlations take over. For the same reason, the quasiparticle weight is not well defined anymore. In Fig. 2, the formation of the local magnetic moment, calculated following Ref. [77], is depicted by the green line. In the weak-coupling regime it lies on top of the Néel phase boundary (dark red curve), which is consistent with a Slater mechanism of the Néel transition in this regime. Remarkably, the LMM curve starts deviating from the Néel phase boundary at $U = 1.0$, exactly when the light red line departs from the

dark red line. This means that at $U > 1.0$ the MIT is no longer determined solely by magnetic fluctuations of itinerant electrons accounted for by the self-energy, as the LMM also starts contributing to the formation of the insulating state. The formation of the LMM also reduces the momentum selectivity in the disappearance of the quasiparticle peak at the $E_F$. Indeed, we find that the LMM curve crosses the AN line at $U \simeq 1.4$ right before the N-AN dichotomy starts being suppressed. This effect can be explained by the fact that the LMM and spatial collective electronic fluctuations are formed by the same electrons. Upon increasing the interaction, more electrons are involved in the formation of the LMM, and thus less electrons remain for the fluctuations. Eventually, when reaching the critical value, the LMM completely screens the fluctuations and the system enters the Mott insulator regime. The formation of the LMM therefore indicates the beginning of the crossover regime separating the weak-coupling Slater part of the phase diagram from the strong-coupling Heisenberg one. The values of the LMM, given in Supplemental Material [72], suggest that the end of the crossover regime occurs upon reaching the critical value of the LMM effectively when the system undergoes the Mott transition.

In conclusion, we have studied the $T$-$U$ phase diagram of the half filled single-orbital Hubbard model on a square lattice. Analyzing the behavior of the momentum-resolved spectral function, we disentangle the contribution of AFM fluctuations and local electronic correlations to the formation of a depletion of spectral weight at the Fermi energy, connecting the weak- and strong-coupling limits. These two limits are separated by a crossover regime that starts when the local magnetic moment is formed and ends at the Mott transition. In this regime, spatial fluctuations are still notable, but the presence of a LMM indicates the emergence of strong local electronic correlations in the system. We identify the weak-coupling region that precedes the crossover with a Slater regime. There, the MIT is solely governed by AFM fluctuations, which results in a momentum-selective formation of the $E_F$ minimum with a pronounced N-AN dichotomy increasing upon increasing interaction. In the intermediate-coupling (crossover) regime, increasing $U$ enhances the value of the LMM and thus reduces the N-AN dichotomy that eventually disappears upon entering the Mott phase. Finally, the Mott phase can be associated with the Heisenberg regime of local magnetic moments. Indeed, we have found that the Mott transition occurs when the LMM reaches a critical value. The simultaneous disappearance of the quasiparticle peak along the Fermi surface at the Mott transition additionally illustrates the governing role of local electronic correlations for the physics of the system. As expected, in the Heisenberg regime, the Néel transition is driven by a decrease in temperature, which separates the Mott phase into paramagnetic and AFM states. This Letter bridges between the weak- and strong-coupling pictures of the 2D Hubbard model on the square lattice at half filling by disentangling the interplay among the different underlying mechanisms.

We thank A. I. Lichtenstein and A. Georges for useful comments and discussions. We acknowledge support from IDRIS/GENCI Orsay under Project No. A0130901393 and the help of the CPHT computer support team.

[1] J. C. Slater, Magnetic effects and the Hartree-Fock equation, Phys. Rev. **82**, 538 (1951).
[2] N. F. Mott, *Metal-Insulator Transitions* (Taylor & Francis, London, 1974).
[3] G. Rohringer and A. Toschi, Impact of nonlocal correlations over different energy scales: A dynamical vertex approximation study, Phys. Rev. B **94**, 125144 (2016).
[4] Masatoshi Imada, Atsushi Fujimori, and Yoshinori Tokura, Metal-insulator transitions, Rev. Mod. Phys. **70**, 1039 (1998).
[5] P. W. Anderson, New approach to the theory of superexchange interactions, Phys. Rev. **115**, 2 (1959).
[6] K. A. Chao, J. Spałek, and A. M. Oleś, Degenerate perturbation theory and its application to the Hubbard model, Phys. Lett. A **64**, 163 (1977).
[7] K. A. Chao, J. Spałek, and A. M. Oleś, Kinetic exchange interaction in a narrow S-band, J. Phys. C **10**, L271 (1977).
[8] A. H. MacDonald, S. M. Girvin, and D. Yoshioka, $(t/U)$ expansion for the Hubbard model, Phys. Rev. B **37**, 9753 (1988).
[9] J. Spałek, $t - J$ model then and now: A personal perspective from the pioneering times, Acta Phys. Pol. A **111**, 409 (2007).
[10] Antoine Georges, Gabriel Kotliar, Werner Krauth, and Marcelo J. Rozenberg, Dynamical mean-field theory of strongly correlated fermion systems and the limit of infinite dimensions, Rev. Mod. Phys. **68**, 13 (1996).
[11] M. H. Hettler, A. N. Tahvildar-Zadeh, M. Jarrell, T. Pruschke, and H. R. Krishnamurthy, Nonlocal dynamical correlations of strongly interacting electron systems, Phys. Rev. B **58**, R7475 (1998).
[12] A. I. Lichtenstein and M. I. Katsnelson, Antiferromagnetism and $d$-wave superconductivity in cuprates: A cluster dynamical mean-field theory, Phys. Rev. B **62**, R9283 (2000).
[13] Gabriel Kotliar, Sergej Y. Savrasov, Gunnar Pálsson, and Giulio Biroli, Cellular dynamical mean field approach to strongly correlated systems, Phys. Rev. Lett. **87**, 186401 (2001).
[14] T. A. Maier, Mark Jarrell, Thomas Pruschke, and Matthias Hettler, Quantum cluster theories, Rev. Mod. Phys. **77**, 1027 (2005).
[15] A.-M. S. Tremblay, B. Kyung, and D. Sénéchal, Pseudogap and high-temperature superconductivity from weak to strong coupling. Towards a quantitative theory (Review Article), Low Temp. Phys. **32**, 424 (2006).

[16] G. Kotliar, S. Y. Savrasov, K. Haule, V. S. Oudovenko, O. Parcollet, and C. A. Marianetti, Electronic structure calculations with dynamical mean-field theory, Rev. Mod. Phys. **78**, 865 (2006).
[17] H. Park, K. Haule, and G. Kotliar, Cluster dynamical mean field theory of the Mott transition, Phys. Rev. Lett. **101**, 186403 (2008).
[18] Malte Harland, Mikhail I. Katsnelson, and Alexander I. Lichtenstein, Plaquette valence bond theory of high-temperature superconductivity, Phys. Rev. B **94**, 125133 (2016).
[19] L. Fratino, P. Sémon, M. Charlebois, G. Sordi, and A.-M. S. Tremblay, Signatures of the Mott transition in the antiferromagnetic state of the two-dimensional Hubbard model, Phys. Rev. B **95**, 235109 (2017).
[20] G. Rohringer, H. Hafermann, A. Toschi, A. A. Katanin, A. E. Antipov, M. I. Katsnelson, A. I. Lichtenstein, A. N. Rubtsov, and K. Held, Diagrammatic routes to nonlocal correlations beyond dynamical mean field theory, Rev. Mod. Phys. **90**, 025003 (2018).
[21] Ya. S. Lyakhova, G. V. Astretsov, and A. N. Rubtsov, The mean-field concept and post-DMFT methods in the contemporary theory of correlated systems, Phys. Usp. **193**, 825 (2023); Phys. Usp. **66**, 775 (2023).
[22] S. Biermann, F. Aryasetiawan, and A. Georges, First-principles approach to the electronic structure of strongly correlated systems: Combining the *GW* approximation and dynamical mean-field theory, Phys. Rev. Lett. **90**, 086402 (2003).
[23] Ping Sun and Gabriel Kotliar, Many-body approximation scheme beyond GW, Phys. Rev. Lett. **92**, 196402 (2004).
[24] Thomas Ayral, Philipp Werner, and Silke Biermann, Spectral properties of correlated materials: Local vertex and nonlocal two-particle correlations from combined *GW* and dynamical mean field theory, Phys. Rev. Lett. **109**, 226401 (2012).
[25] Thomas Ayral, Silke Biermann, and Philipp Werner, Screening and nonlocal correlations in the extended Hubbard model from self-consistent combined *GW* and dynamical mean field theory, Phys. Rev. B **87**, 125149 (2013).
[26] Li Huang, Thomas Ayral, Silke Biermann, and Philipp Werner, Extended dynamical mean-field study of the Hubbard model with long-range interactions, Phys. Rev. B **90**, 195114 (2014).
[27] L. Boehnke, F. Nilsson, F. Aryasetiawan, and P. Werner, When strong correlations become weak: Consistent merging of *GW* and DMFT, Phys. Rev. B **94**, 201106(R) (2016).
[28] Thomas Ayral, Silke Biermann, Philipp Werner, and Lewin Boehnke, Influence of Fock exchange in combined many-body perturbation and dynamical mean field theory, Phys. Rev. B **95**, 245130 (2017).
[29] A. N. Rubtsov, M. I. Katsnelson, and A. I. Lichtenstein, Dual fermion approach to nonlocal correlations in the Hubbard model, Phys. Rev. B **77**, 033101 (2008).
[30] A. N. Rubtsov, M. I. Katsnelson, A. I. Lichtenstein, and A. Georges, Dual fermion approach to the two-dimensional Hubbard model: Antiferromagnetic fluctuations and Fermi arcs, Phys. Rev. B **79**, 045133 (2009).
[31] H. Hafermann, G. Li, A. N. Rubtsov, M. I. Katsnelson, A. I. Lichtenstein, and H. Monien, Efficient perturbation theory for quantum lattice models, Phys. Rev. Lett. **102**, 206401 (2009).
[32] Sergei Iskakov, Andrey E. Antipov, and Emanuel Gull, Diagrammatic Monte Carlo for dual fermions, Phys. Rev. B **94**, 035102 (2016).
[33] Jan Gukelberger, Evgeny Kozik, and Hartmut Hafermann, Diagrammatic Monte Carlo approach for diagrammatic extensions of dynamical mean-field theory: Convergence analysis of the dual fermion technique, Phys. Rev. B **96**, 035152 (2017).
[34] Sergey Brener, Evgeny A. Stepanov, Alexey N. Rubtsov, Mikhail I. Katsnelson, and Alexander I. Lichtenstein, Dual fermion method as a prototype of generic reference-system approach for correlated fermions, Ann. Phys. (Amsterdam) **422**, 168310 (2020).
[35] A. N. Rubtsov, M. I. Katsnelson, and A. I. Lichtenstein, Dual boson approach to collective excitations in correlated fermionic systems, Ann. Phys. (Amsterdam) **327**, 1320 (2012).
[36] Erik G. C. P. van Loon, Alexander I. Lichtenstein, Mikhail I. Katsnelson, Olivier Parcollet, and Hartmut Hafermann, Beyond extended dynamical mean-field theory: Dual boson approach to the two-dimensional extended Hubbard model, Phys. Rev. B **90**, 235135 (2014).
[37] E. A. Stepanov, E. G. C. P. van Loon, A. A. Katanin, A. I. Lichtenstein, M. I. Katsnelson, and A. N. Rubtsov, Self-consistent dual boson approach to single-particle and collective excitations in correlated systems, Phys. Rev. B **93**, 045107 (2016).
[38] E. A. Stepanov, A. Huber, E. G. C. P. van Loon, A. I. Lichtenstein, and M. I. Katsnelson, From local to nonlocal correlations: The dual boson perspective, Phys. Rev. B **94**, 205110 (2016).
[39] Evgeny A. Stepanov, Lars Peters, Igor S. Krivenko, Alexander I. Lichtenstein, Mikhail I. Katsnelson, and Alexey N. Rubtsov, Quantum spin fluctuations and evolution of electronic structure in cuprates, npj Quantum Mater. **3**, 54 (2018).
[40] L. Peters, E. G. C. P. van Loon, A. N. Rubtsov, A. I. Lichtenstein, M. I. Katsnelson, and E. A. Stepanov, Dual boson approach with instantaneous interaction, Phys. Rev. B **100**, 165128 (2019).
[41] M. Vandelli, V. Harkov, E. A. Stepanov, J. Gukelberger, E. Kozik, A. Rubio, and A. I. Lichtenstein, Dual boson diagrammatic Monte Carlo approach applied to the extended Hubbard model, Phys. Rev. B **102**, 195109 (2020).
[42] A. Toschi, A. A. Katanin, and K. Held, Dynamical vertex approximation: A step beyond dynamical mean-field theory, Phys. Rev. B **75**, 045118 (2007).
[43] A. A. Katanin, A. Toschi, and K. Held, Comparing pertinent effects of antiferromagnetic fluctuations in the two- and three-dimensional Hubbard model, Phys. Rev. B **80**, 075104 (2009).
[44] Anna Galler, Patrik Thunström, Patrik Gunacker, Jan M. Tomczak, and Karsten Held, *Ab initio* dynamical vertex approximation, Phys. Rev. B **95**, 115107 (2017).
[45] Anna Galler, Josef Kaufmann, Patrik Gunacker, Matthias Pickem, Patrik Thunström, Jan M. Tomczak, and Karsten Held, Towards *ab initio* calculations with the dynamical vertex approximation, J. Phys. Soc. Jpn. **87**, 041004 (2018).

[46] Josef Kaufmann, Christian Eckhardt, Matthias Pickem, Motoharu Kitatani, Anna Kauch, and Karsten Held, Self-consistent ladder dynamical vertex approximation, Phys. Rev. B **103**, 035120 (2021).
[47] Thomas Ayral and Olivier Parcollet, Mott physics and spin fluctuations: A unified framework, Phys. Rev. B **92**, 115109 (2015).
[48] Thomas Ayral and Olivier Parcollet, Mott physics and spin fluctuations: A functional viewpoint, Phys. Rev. B **93**, 235124 (2016).
[49] J. Vučičević, T. Ayral, and O. Parcollet, TRILEX and $GW+$EDMFT approach to $d$-wave superconductivity in the Hubbard model, Phys. Rev. B **96**, 104504 (2017).
[50] Thomas Ayral, Jaksa Vučičević, and Olivier Parcollet, Fierz convergence criterion: A controlled approach to strongly interacting systems with small embedded clusters, Phys. Rev. Lett. **119**, 166401 (2017).
[51] E. A. Stepanov, V. Harkov, and A. I. Lichtenstein, Consistent partial bosonization of the extended Hubbard model, Phys. Rev. B **100**, 205115 (2019).
[52] V. Harkov, M. Vandelli, S. Brener, A. I. Lichtenstein, and E. A. Stepanov, Impact of partially bosonized collective fluctuations on electronic degrees of freedom, Phys. Rev. B **103**, 245123 (2021).
[53] Matteo Vandelli, Josef Kaufmann, Mohammed El-Nabulsi, Viktor Harkov, Alexander I. Lichtenstein, and Evgeny A. Stepanov, Multi-band D-TRILEX approach to materials with strong electronic correlations, SciPost Phys. **13**, 036 (2022).
[54] Nikolai V. Prokof'ev and Boris V. Svistunov, Polaron problem by diagrammatic quantum Monte Carlo, Phys. Rev. Lett. **81**, 2514 (1998).
[55] E. Kozik, K. Van Houcke, E. Gull, L. Pollet, N. Prokof'ev, B. Svistunov, and M. Troyer, Diagrammatic Monte Carlo for correlated fermions, Europhys. Lett. **90**, 10004 (2010).
[56] Riccardo Rossi, Determinant diagrammatic Monte Carlo algorithm in the thermodynamic limit, Phys. Rev. Lett. **119**, 045701 (2017).
[57] Fedor Šimkovic and Evgeny Kozik, Determinant Monte Carlo for irreducible Feynman diagrams in the strongly correlated regime, Phys. Rev. B **100**, 121102(R) (2019).
[58] Aaram J. Kim, Fedor Simkovic, and Evgeny Kozik, Spin and charge correlations across the metal-to-insulator crossover in the half-filled 2D Hubbard model, Phys. Rev. Lett. **124**, 117602 (2020).
[59] Thomas Schäfer *et al.*, Tracking the footprints of spin fluctuations: A multimethod, multimessenger study of the two-dimensional Hubbard model, Phys. Rev. X **11**, 011058 (2021).
[60] J. P. F. LeBlanc *et al.*, (Simons Collaboration on the Many-Electron Problem), Solutions of the two-dimensional Hubbard model: Benchmarks and results from a wide range of numerical algorithms, Phys. Rev. X **5**, 041041 (2015).
[61] Jan Gukelberger, Li Huang, and Philipp Werner, On the dangers of partial diagrammatic summations: Benchmarks for the two-dimensional Hubbard model in the weak-coupling regime, Phys. Rev. B **91**, 235114 (2015).
[62] John Hubbard, Electron correlations in narrow energy bands, Proc. R. Soc. A **276**, 238 (1963).
[63] Evgeny A. Stepanov, Yusuke Nomura, Alexander I. Lichtenstein, and Silke Biermann, Orbital isotropy of magnetic fluctuations in correlated electron materials induced by Hund's exchange coupling, Phys. Rev. Lett. **127**, 207205 (2021).
[64] E. A. Stepanov, V. Harkov, M. Rösner, A. I. Lichtenstein, M. I. Katsnelson, and A. N. Rudenko, Coexisting charge density wave and ferromagnetic instabilities in monolayer InSe, npj Comput. Mater. **8**, 118 (2022).
[65] M. Vandelli, J. Kaufmann, V. Harkov, A. I. Lichtenstein, K. Held, and E. A. Stepanov, Extended regime of metastable metallic and insulating phases in a two-orbital electronic system, Phys. Rev. Res. **5**, L022016 (2023).
[66] Evgeny A. Stepanov, Eliminating orbital selectivity from the metal-insulator transition by strong magnetic fluctuations, Phys. Rev. Lett. **129**, 096404 (2022).
[67] M. Vandelli, A. Galler, A. Rubio, A. I. Lichtenstein, S. Biermann, and E. A. Stepanov, Doping-dependent charge- and spin-density wave orderings in a monolayer of Pb adatoms on Si(111), npj Quantum Mater. **9**, 19 (2024).
[68] Evgeny A. Stepanov and Silke Biermann, Can orbital-selective Néel transitions survive strong nonlocal electronic correlations?, arXiv:2305.16730 [Phys. Rev. Lett. (to be published)].
[69] Evgeny A. Stepanov, Maria Chatzieleftheriou, Niklas Wagner, and Giorgio Sangiovanni, Interconnected renormalization of Hubbard bands and Green's function zeros in Mott insulators induced by strong magnetic fluctuations, arXiv:2402.02814.
[70] Evgeny A. Stepanov, Matteo Vandelli, Alexander I. Lichtenstein, and Frank Lechermann, Charge density wave ordering in $NdNiO_2$: Effects of multiorbital nonlocal correlations, npj Comput. Mater **10**, 108 (2024).
[71] Josef Kaufmann and Karsten Held, ANA_CONT: python package for analytic continuation, arXiv:2105.11211.
[72] See Supplemental Material at http://link.aps.org/supplemental/10.1103/PhysRevLett.132.236504 for (I) a discussion of the momentum-resolved spectral function in single-site DMFT, (II) a description of the mirroring effect observed in the momentum-resolved spectral function in D-TRILEX, (III) a discussion of the LMM formation, and (IV) an illustration of the self-energy behavior, which includes Refs. [73,74].
[73] N. E. Bickers and D. J. Scalapino, Conserving approximations for strongly fluctuating electron systems. I. Formalism and calculational approach, Ann. Phys. (N.Y.) **193**, 206 (1989).
[74] A. I. Lichtenstein and M. I. Katsnelson, *Ab initio* calculations of quasiparticle band structure in correlated systems: LDA++ approach, Phys. Rev. B **57**, 6884 (1998).
[75] Arata Tanaka, Metal-insulator transition in the two-dimensional Hubbard model: Dual fermion approach with Lanczos exact diagonalization, Phys. Rev. B **99**, 205133 (2019).
[76] Fedor Šimkovic, J. P. F. LeBlanc, Aaram J. Kim, Youjin Deng, N. V. Prokof'ev, B. V. Svistunov, and Evgeny Kozik, Extended crossover from a Fermi liquid to a quasiantiferromagnet in the half-filled 2D Hubbard model, Phys. Rev. Lett. **124**, 017003 (2020).
[77] E. A. Stepanov, S. Brener, V. Harkov, M. I. Katsnelson, and A. I. Lichtenstein, Spin dynamics of itinerant electrons: Local magnetic moment formation and Berry phase, Phys. Rev. B **105**, 155151 (2022).